Polymers |*Hot Paper*|

The Effect of α-Branched Side Chains on the Structural and Opto-Electronic Properties of Poly(Diketopyrrolopyrrole-*alt*-Terthiophene)

Bart W. H. Saes,[a] Martijn M. Wienk,[a] and René A. J. Janssen*[a, b]

Abstract: Introducing solubilizing α-branched alkyl chains on a poly(diketopyrrolopyrrole-*alt*-terthiophene) results in a dramatic change of the structural, optical, and electronic properties compared to the isomeric polymer carrying β-branched alkyl side chains. When branched at the α-position the alkyl substituent creates a steric hindrance that reduces the tendency of the polymer to π–π stack and endows the material with a much higher solubility in common organic solvents. The wider π–π stacking and reduced tendency to crystallize, evidenced from grazing-incidence wide-angle X-ray scattering, result in a wider optical band gap in the solid state. In solar cells with a fullerene acceptor, the α-branched isomer affords a higher open-circuit voltage, but an overall lower power conversion efficiency as a result of a too well-mixed nanomorphology. Due its reduced π–π stacking, the α-branched isomer fluoresces and affords near-infrared light-emitting diodes emitting at 820 nm.

Introduction

Semiconducting polymers can be made solution-processable by grafting solubilizing alkyl groups onto the π-conjugated backbone.[1–4] The solubilizing groups serve an important role in defining the three-dimensional structure in solid state thin films, but generally do not have a direct effect on the opto-electronic properties, other than modulating chain–chain interactions. In essence, there is no real need for the side chains after the microscopic organization of the polymer materials has been established.

For saturated alkyl side chains, the only design variables are their length and branching. Compared to linear side chains, alkyl chains that comprise branching points at tertiary carbon atoms provide the polymer with a strongly reduced tendency to aggregate, and consequently a higher degree of solubility, and reduced melting point.[1] The most commonly investigated branched side chains, have a branching point at the β-carbon relative to the π-conjugated backbone, or at a carbon atom further away. For several polymers, a shift of the branching point position away from the polymer backbone resulted in tighter π–π stacking.[3,5–8] However, this is not always coupled to an increased charge carrier mobility as measured in organic field-effect transistors. The alkyl chain can also influence the preferred orientation (edge-on versus face-on) of the π-conjugated main chain with respect to the substrate after depositing the polymers from solution.[6,7,9]

For diketopyrrolopyrrole (DPP) based polymers, branched side chains reduce the strong π–π stacking interactions and are essential to afford solution-processable polymers.[4,10–13] Bulky side chains on the DPP unit reduce aggregation or even completely prevent it.[14] For DPP-based polymers similar trends have been reported as for other conjugated polymers when the distance between the branching point and the main chain is increased.[15] In this study, we investigate the effect of moving the branching point of the alkyl side chains on the DPP unit from the β-carbon to the α-carbon in a polymer (PDPP3T) in which the DPP unit alternates with a terthiophene (3T) moiety along the main chain. The two isomeric polymers 1′HD-PDPP3T and 2′HD-PDPP3T are shown in Figure 1.

By positioning the branching point closer to the conjugated backbone, the π–π stacking of the DPP units must be affected because the two alkyl chains that emerge from the branching point cannot be coplanar with the polymer main chain. In fact, they are expected to be pointing up and down from the π-conjugated plane because of steric hindrance with the nearby oxygen and sulfur atoms. As a result, the solubility of the polymer will be enhanced. In the remainder the synthesis and optical and electronic properties of 1′HD-PDPP3T are discussed and compared to that of 2′HD-PDPP3T.

[a] *B. W. H. Saes, Dr. M. M. Wienk, Prof. R. A. J. Janssen*
Molecular Materials and Nanosystems and Institute for Complex Molecular Systems, Eindhoven University of Technology
5600 MB Eindhoven (The Netherlands)
E-mail: r.a.j.janssen@tue.nl

[b] *Prof. R. A. J. Janssen*
Dutch Institute for Fundamental Energy Research
De Zaale 20, 5612 AJ Eindhoven (The Netherlands)

Supporting information and the ORCID identification number(s) for the author(s) of this article can be found under: https://doi.org/10.1002/chem.202001722.

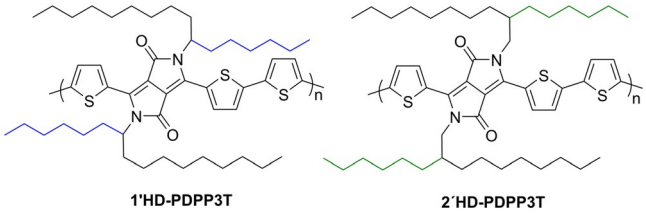

Figure 1. Structures of 1′HD-PDPP3T and 2′HD-PDPP3T with the branching points of the hexyldecyl side chains on the α (1′) and β (2′) positions.

Results and Discussion

Synthesis

The synthetic route to 1′HD-PDPP3T is shown in Scheme 1. To synthesize 7-bromohexadecane, the Grignard reagent of 1-bromohexane was reacted with decanal to afford hexadecan-7-ol (**1**) in 81% yield. Hexadecane-7-ol (**1**) was subsequently converted into 7-bromohexadecane (**2**) through an Appel reaction in about 66% yield. The obtained crude oil was used to alkylate 3,6-di(thiophen-2-yl)-2,5-dihydropyrrolo[3,4-*c*]pyrrole-1,4-dione (**3**) under standard alkylation conditions[16] to afford **4** in a very low yield of 2.1%.

Attempts were made to improve the yield of the alkylation reaction by extracting the product from the reaction with heptane and feeding more 7-bromohexadecane to the reaction mixture, yet the yield remained 2.1%. This yield is significantly lower than the yields of about 40% that are usually obtained in alkylation of **3** by linear 1-bromoalkanes or 1-bromoalkanes branched in the 2′-position. We reason that the yield is low because deprotonated **3** is a sterically hindered nucleophile and nucleophilic substitution at a secondary carbon atom is not favored. Competing degradation reactions such as elimination, are less affected by this change in the nature of the bromoalkane. Possibly, it is this low yield that has previously discouraged investigations on 1′-branched DPP chromophores. Bromination of **4** by *N*-bromosuccinimide (NBS) afforded monomer **5** in about 75% yield. Monomer **5** was then polymerized with 2,5-bis(trimethylstannyl)thiophene in a palladium-catalyzed Stille reaction to afford 1′HD-PDPP3T, which was isolated by Soxhlet extraction with hexane. The solubility of 1′HD-PDPP3T in hexane, strongly contrasts with that of 2′HD-PDPP3T for which 1,1,2,2-tetrachloroethane (TCE) is needed to extract the higher molecular weight fractions from the polymerization reaction mixture.[17,18] A PDPP3T derivative with much shorter 1′-branched side chains (1′-ethylpropyl), however, turned out to be insoluble. A sample of 2′HD-PDPP3T previously prepared was used compare the two materials.

Gel permeation chromatography (GPC) at 140 °C using *ortho*-dichlorobenzene (*o*-DCB) as eluent revealed that the number average molecular weights (M_n) of 1′HD-PDPP3T (83 kDa) and 2′HD-PDPP3T (67 kDa) are high and have polydispersity (*Đ*) of 2.8 and 2.1 (Table 1).

Table 1. Molecular weights.

	M_n (kDa)	M_w (kDa)	*Đ*
1′HD-PDPP3T	83	232	2.8
2′HD-PDPP3T	67	143	2.1

Optical, electronic and structural properties

Figure 2 shows the temperature-dependent UV-vis-NIR absorption spectra of 1′HD-PDPP3T and 2′HD-PDPP3T in TCE. At room temperature, 1′HD-PDPP3T shows a strong, unstructured absorption band maximizing at 693 nm, while 2′HD-PDPP3T exhibits a structured band with a maximum at 821 nm and a shoulder at around 620 nm. The structured optical absorption spectrum of 2′HD-PDPP3T originates from π–π stacking interactions between polymer chains and is typical for aggregated DPP polymers. In contrast, for 1′HD-PDPP3T, the unstructured absorption gives suggests that the polymer chains are molecularly dissolved. Upon raising the temperature in TCE, both absorption spectra exhibit a blue shift, but the details are different. For 1′HD-PDPP3T there is a shift of the absorption maximum from 693 to 668 nm, but the onset of the spectrum remains at about 800 nm (Figure 2a). These are the signatures of a conjugated polymer chain that becomes more disordered at higher temperatures by reducing its co-planarity via increased dihedral angles between adjacent heterocycles. The reduced co-planarity reduces the effective conjugation length and creates a concomitant blue shifted absorption maximum.[19,20] The constant onset at 800 nm signifies that some chain segments remain essentially co-planar, but their number reduces as the intensity becomes less. On the other hand, for 2′HD-PDPP3T

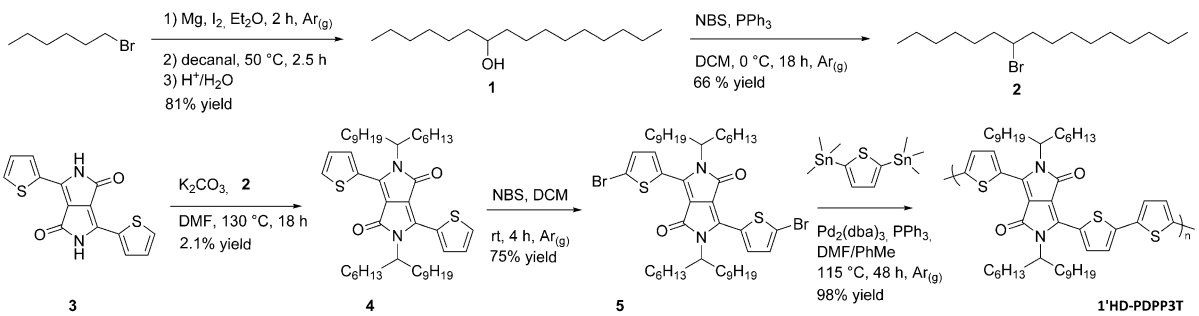

Scheme 1. Synthesis of 1′HD-PDPP3T.

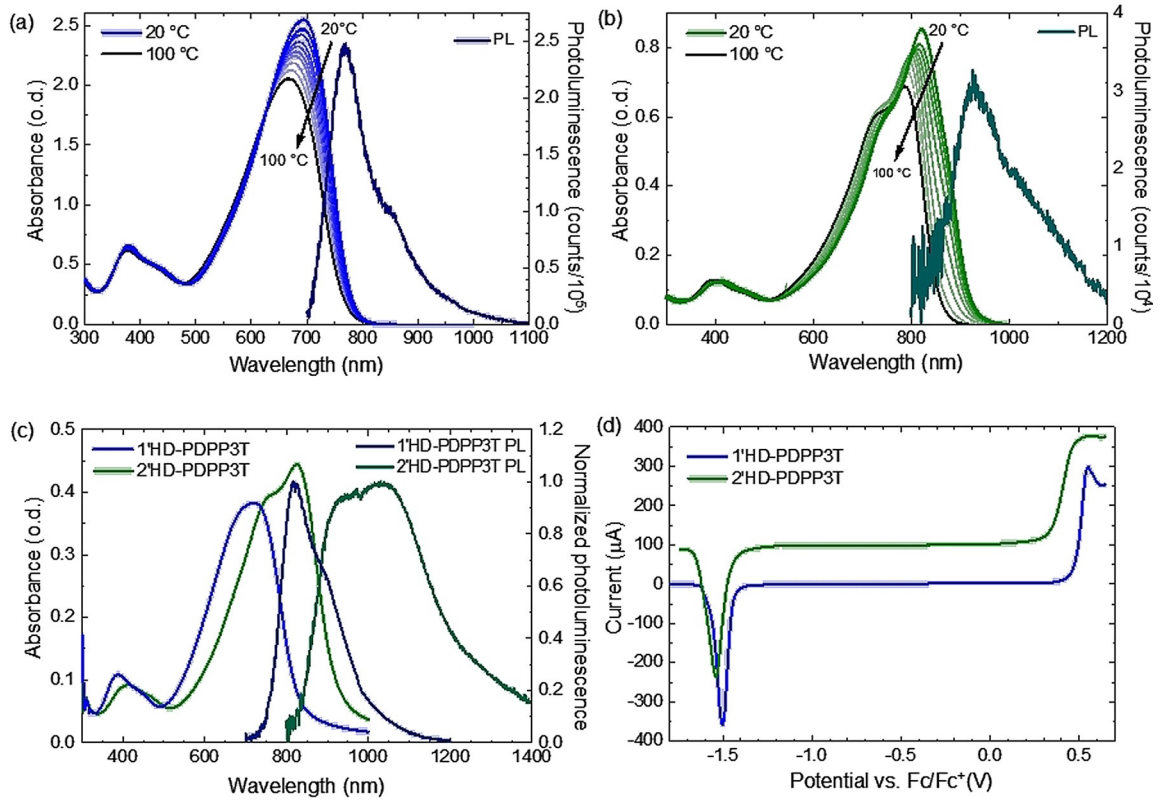

Figure 2. (a) Temperature-dependent UV-vis-NIR absorption spectra of 1′HD-PDPP3T in TCE and photoluminescence spectrum of 1′HD-PDPP3T in TCE at room temperature with excitation at 700 nm. (b) Temperature dependent UV-vis-NIR absorption spectra of 2′HD-PDPP3T in TCE and photoluminescence spectrum of 2′HD-PDPP3T in TCE at room temperature with excitation at 800 nm. (c) UV-vis-NIR spectra of films (40 nm) of 1′HD-PDPP3T and 2′HD-PDPP3T and their corresponding thin film photoluminescence spectra recorded with excitation at 600 and 700 nm, respectively. (d) Square-wave voltammetry of films of 1′HD-PDPP3T and 2′HD-PDPP3T on a Pt wire in an acetonitrile electrolyte. Voltage is versus Fc/Fc^+. The two curves are offset vertically for clarity.

both the maximum (from 821 to 787 nm) and the onset (from about 950 to 900 nm) shift when increasing the temperature (Figure 2b). The intensity ratio of the main absorption band and the shoulder at lower wavelength also decreases. These are the clear signatures of a reduced aggregation when the temperature increases. The fact that even at 100 °C in TCE, the UV-vis-NIR spectra of 2′HD-PDPP3T show a structured absorption band, indicates that the chains are not fully molecularly dissolved under these conditions. 1′HD-PDPP3T and 2′HD-PDPP3T both exhibit weak fluorescence in the (near) infrared region at around 800 nm for 1′HD-PDPP3T and around 900 nm for 2′HD-PDPP3T when dissolved in chloroform (Figure 2a, b).

The strong differences between the absorption spectra of 1′HD-PDPP3T and 2′HD-PDPP3T observed in solution remain in thin films (Figure 2c). The optical band gaps (E_g) determined at the onsets of the absorption bands are 1.50 eV for 1′HD-PDPP3T and 1.32 eV for 2′HD-PDPP3T. The significant difference shows that also in the solid state the interaction between 1′HD-PDPP3T chains is much less than for 2′HD-PDPP3T chains. By comparing the spectra in Figure 2, the red shift occurring between solution and thin film is somewhat larger than for 1′HD-PDPP3T than for 2′HD-PDPP3T. This can be understood by considering that 2′HD-PDPP3T chains are aggregated under both conditions. In thin films 1′HD-PDPP3T and 2′HD-PDPP3T also exhibit weak fluorescence (Figure 2c).

Square wave voltammetry (SWV) of thin films emerged in an acetonitrile electrolyte was used to determine the oxidation and reduction potentials (Figure 2d). In SWV, the onsets of the oxidation waves are found at +0.48 V for 1′HD-PDPP3T and +0.34 V for 2′HD-PDPP3T versus ferrocene/ferrocenium (Fc/Fc^+). The reduction potentials are even closer and at −1.45 and −1.46 V, respectively. Using a value of $E(Fc/Fc^+) = -4.59$ eV versus vacuum the energies of the HOMO (E_{HOMO}) and LUMO (E_{LUMO}) levels are obtained (Table 2).[21] The electrochemical band gaps ($E_g^{SWV} = E_{LUMO} - E_{HOMO}$) are larger than the optical band gaps by 0.43 and 0.48 eV, respectively in excellent agreement with the average of 0.44 ± 0.02 eV, found for a collection of nineteen different DPP polymers.[21]

The hole mobility of 1′HD-PDPP3T and 2′HD-PDPP3T was determined in planar devices in which the polymers were sandwiched between ITO/PEDOT:PSS and MoO_3/Ag electrodes. The current density (J) vs. voltage (V) characteristics (Figure 3)

Table 2. Optical band gaps, HOMO and LOMO energies, and electrochemical band gaps.

	E_g (eV)	E_{HOMO} (eV)	E_{LUMO} (eV)	E_g^{SWV} (eV)
1′HD-PDPP3T	1.50	−5.07	−3.13	1.93
2′HD-PDPP3T	1.32	−4.93	−3.13	1.80

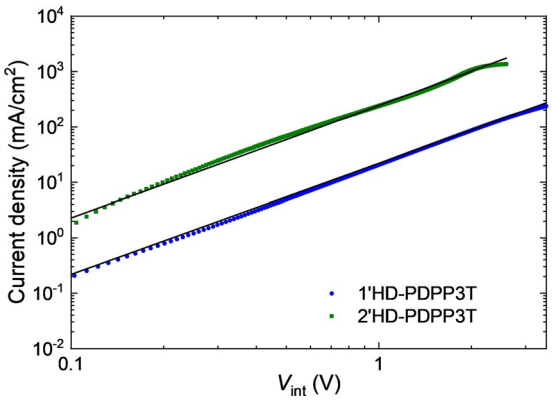

Figure 3. *J–V* characteristics of the hole-only devices for 1′HD-PDPP3T ($L = 275$ nm) and 2′HD-PDPP3T ($L = 310$ nm). The solid lines represent fits to the Murgatroyd relation, the symbols are experimental data. The voltage was corrected for the built-in potential and series resistance.

were fitted to the Murgatroyd relation for space charge limited current with field-dependent mobility: $J = (9/8)\varepsilon_0\varepsilon_r\mu_0(V^2L^{-3})\exp[0.89\gamma(VL^{-1})^{1/2}]$,[22,23] with ε_0 the vacuum permittivity, ε_r the relative permittivity of the polymers (approximated to be 3), μ_0 the zero-field mobility, L the thickness of the organic layer, and γ the field-activation factor. The voltage was corrected for built-in potential and series resistance. The hole mobility at an electric field of 10^5 V cm^{-1} is about 1.6×10^{-3} cm^{2}V^{-1}s^{-1} for 1′HD-PDPP3T and 2.6×10^{-2} cm^{2}V^{-1}s^{-1} for 2′HD-PDPP3T and therefore more than one order of magnitude larger for 2′HD-PDPP3T.

Two-dimensional grazing-incidence wide-angle X-ray scattering (2D-GIWAXS) measurements on neat films of 1′HD-PDPP3T and 2′HD-PDPP3T are shown in Figure 4 together with the corresponding out-of-plane and in-plane line cut profiles. 2′HD-PDPP3T shows a lamellar stacking peak at $q = 0.32$ Å^{-1} and broad π–π stacking signal at $q = 1.70$ Å^{-1} in the in-plane and out-of-plane directions. These correspond to distances of 19.7 Å and 3.70 Å, respectively and are in accordance with previous studies on this polymer.[18] For 1′HD-PDPP3T, the scattering signal intensity is much lower and shows a vague lamellar stacking peak at $q = 0.36$ Å^{-1} (17.4 Å) and π–π stacking signal at $q = 1.44$ Å^{-1} (4.36 Å). These results indicate that 1′HD-PDPP3T has a lesser tendency to crystallize than 2′HD-PDPP3T. The result that the lamellar spacing is slightly reduced in 1′HD-PDPP3T compared to 2′HD-PDPP3T, indicates that the alkyl side chains in 1′HD-PDPP3T are more orthogonal to the main chain. The longer π–π stacking distance of 4.36 Å for 1′HD-PDPP3T compared to 3.70 Å for 2′HD-PDPP3T shows that α-branching effectively reduces the tendency for π–π stacking, enforced by an out of plane orientation of the alkyl side chains. The large difference in π–π stacking distance is consistent with the large difference in hole mobility.

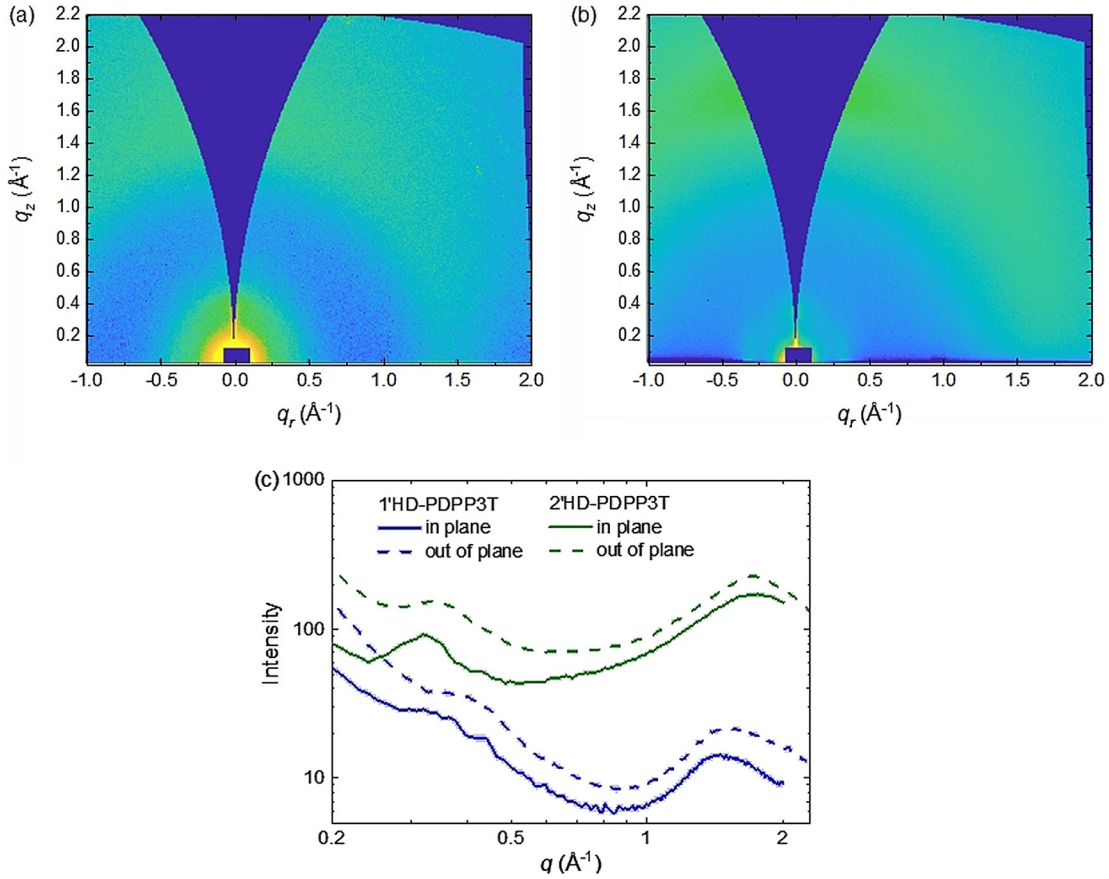

Figure 4. 2D-GIWAXS patterns of neat (a) 1′HD-PDPP3T and (b) 2′HD-PDPP3T films. (c) Corresponding in-plane and out-of-plane line cut profiles as function of the scattering vector *q*.

Photovoltaic properties

Solar cells were made using 1′HD-PDPP3T as donor and [6,6]-phenyl C_{71} butyric acid methyl ester ($PC_{71}BM$) as acceptor in a device configuration in which the photoactive layer is sandwiched between a transparent front electrode consisting of indium tin oxide (ITO) covered with poly(3,4-ethylenedioxythiophene) polystyrene sulfonate (PEDOT:PSS) and an opaque back contact of LiF and Al. Figure 5 shows the current density–voltage (*J-V*) characteristics and external quantum efficiency (EQE) spectra of the cells in which 1′HD-PDPP3T and $PC_{71}BM$ are mixed in a 1:2 weight ratio. Layers were cast from chloroform using 2% of diphenyl ether (DPE) as co-solvent. They are compared to previously reported 2′HD-PDPP3T:$PC_{71}BM$ cells (1:2 w/w). The photovoltaic parameters, listed in Table 3, show that 1′HD-PDPP3T achieves a lower short-circuit current (J_{sc}) and a higher open-circuit voltage (V_{oc}). The EQE spectra reveal that for 1′HD-PDPP3T cells, the J_{sc} is reduced because of the wider optical band gap compared to 2′HD-PDPP3T, but also because of a lower EQE, which indicates less efficient charge generation and collection. The V_{oc}, however, increases by 0.22 V. This is more than the expected increase of 0.14 V, which is the difference between the E_{HOMO} of the two polymers (Table 2). The FF of the 1′HD-PDPP3T cells (0.38) is significantly lower than that of 2′HD-PDPP3T (0.69). The low FF relates to poor charge transport for 1′HD-PDPP3T of which the hole mobility is one order of magnitude lower than for 2′HD-PDPP3T. The reduced mobility gives rise to more non-geminate charge recombination and explains the low FF.[24] Because 1′HD-PDPP3T is much less crystalline than 2′HD-PDPP3T and the π–π stacking distance is larger, it is not surprising that the FF is lower because both factors reduce the carrier mobility. The *J–V* curve of the 1′HD-PDPP3T cell (Figure 5a) shows an increase in photocurrent when the voltage bias is reduced. This is a signature of charges that can only be collected by applying an electric field. In total the power conversion efficiency (PCE) of the 1′HD-PDPP3T:$PC_{71}BM$ cell (2.35%) is significantly lower than that of the 2′HD-PDPP3T:$PC_{71}BM$ cell (7.1%).[17]

It is of interest to compare the minimal photon energy loss (E_{loss}) incurred in the solar cells based on 1′HD-PDPP3T and 2′HD-PDPP3T. This parameter is defined as $E_{loss}=E_g-qV_{oc}$ and equals the minimal energy loss photogenerated charges incur from the initial photon energy. For 1′HD-PDPP3T:$PC_{71}BM$ cells, E_{loss} is 0.59 eV, while it is 0.65 eV for 2′HD-PDPP3T:$PC_{71}BM$ cells. While the difference is small, it is close to the empirical threshold of $E_{loss}=0.60$ eV, required for efficient charge generation.[25] Close to this threshold small differences become important and in this case it may contribute to the reduced EQE for the 1′HD-PDPP3T:$PC_{71}BM$ cells.

A clear advantage of the enhanced solubility of 1′HD-PDPP3T in common solvents is that it enables casting the photoactive layer from non-chlorinated solvents. In contrast, 2′HD-PDPP3T can only be processed from chloroform or TCE. Figure 5 shows the device characteristics of 1′HD-

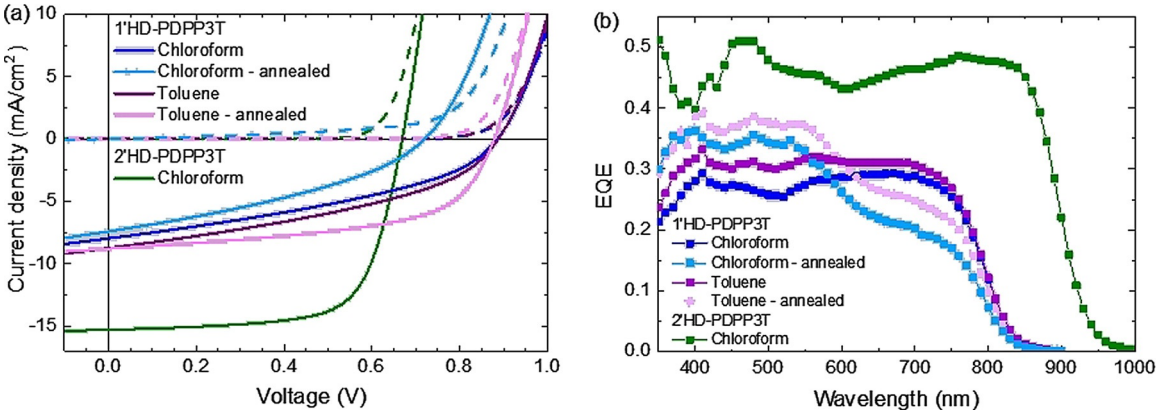

Figure 5. (a) *J–V* characteristics of 1′HD-PDPP3T:$PC_{71}BM$ and 2′HD-PDPP3T:$PC_{71}BM$ solar cells. Solids line were measured under simulated AM1.5G (100 mW cm^{-2}) illumination and dashed lines were recorded in the dark. (b) Corresponding EQE spectra. Data for 2′HD-PDPP3T:$PC_{71}BM$ were taken ref. [17].

Table 3. Photovoltaic parameters of 1′HD-PDPP3T:$PC_{71}BM$ and 2′HD-PDPP3T:$PC_{71}BM$ solar cells.

	d[a] (nm)	Processing[b]	V_{oc}[a] (V)	FF[a]	$J_{sc,EQE}$[a,c] (mA cm^{-2})	PCE[a,b] (%)
1′HD-PDPP3T	105 ± 1	chloroform	0.89 ± 0.00	0.38 ± 0.00	6.97 ± 0.10	2.35 ± 0.04
1′HD-PDPP3T	83 ± 3	chloroform/150 °C	0.65 ± 0.05	0.33 ± 0.02	7.40 ± 0.04	1.58 ± 0.24
1′HD-PDPP3T	95 ± 1	toluene	0.88 ± 0.00	0.40 ± 0.00	7.78 ± 0.02	2.75 ± 0.04
1′HD-PDPP3T	95 ± 1	toluene/150 °C	0.88 ± 0.01	0.56 ± 0.03	8.00 ± 0.04	3.96 ± 0.05
2′HD-PDPP3T[d]	134	chloroform	0.67	0.69	15.4	7.1

[a] Average values and standard deviations were obtained over 3 devices. [b] For 1′HD-PDPP3T 2% DPE was used as co-solvent; for 2′HD-PDPP3T 7.5% 1,2-dichlorobenzene, annealing was for 30 s when used. [c] J_{sc} was determined from EQE measurements by integration with the AM.15G spectrum. [d] From ref. [17].

PDPP3T:$PC_{71}BM$ cells, cast from toluene using 2% DPE as co-solvent. The device performance and the solar cells parameters (Table 3) are very similar to the cells cast from chloroform. Thermal annealing of the devices cast from toluene/DPE at 150 °C resulted in considerably improved FF as well as a small increase in photocurrent density, improving the overall efficiency to close to 4.0%. Thermal annealing also results in a change of the EQE spectrum which increases for wavelengths below 600 nm but decreases at higher wavelengths. This suggests that annealing increases the contribution of photons absorbed by $PC_{71}BM$, but decreases the contribution from 1′HD-PDPP3T. Thermal annealing at 150 °C of 1′HD-PDPP3T:$PC_{71}BM$ blends cast from chloroform/DPE, gave a similar change in the EQE spectrum, but in this case there was a loss in V_{oc} and FF.

The photovoltaic performance of bulk heterojunction solar cells is strongly related to the morphology of the blend.[26–28] Figure 6 shows transmission electron microscopy (TEM) images of the optimized photoactive layers of 1′HD-PDPP3T:$PC_{71}BM$ and 2′HD-PDPP3T:$PC_{71}BM$ blends. The 2′HD-PDPP3T:$PC_{71}BM$ blend (Figure 6c) shows the well-established fibrillar nanostructure encountered for many DPP-polymer-based solar cells in which a dense network of thin semi-crystalline polymer fibrils is percolating in a continuous matrix that is richer in $PC_{71}BM$ and appears darker in the TEM images as result of the higher density of the fullerene.[29–31] In comparison, the TEM image of the 1′HD-PDPP3T:$PC_{71}BM$ blend cast from chloroform/DPE (Figure 6a) shows much less contrast indicating a more homogenous mixing. Apart from indistinct features with the size of tens of nanometers, the TEM image is virtually structureless, pointing to a well-intermixed nanomorphology. A highly intimate mixed blend is expected to perform poorly for charge separation and transport and leads to enhanced geminate recombination of charges that cannot escape form the interface and enhanced non-geminate recombination when opposite charge carriers meet frequently because pure domains of the donor and acceptor material are virtually absent. As a consequence of the enhanced geminate recombination in 1′HD-PDPP3T:$PC_{71}BM$ blends the EQE of these cells is less that of the 2′HD-PDPP3T:$PC_{71}BM$ cells, while the enhanced non-geminate recombination is reflected in the reduced FF of 0.38 compared to 0.69 and an enhanced voltage bias dependence of the photocurrent seen in the *J*–*V* characteristics.[24] 1′HD-PDPP3T:$PC_{71}BM$ blends cast from toluene/DPE (Figure 6b), show a very similar morphology and also the photovoltaic parameters (Table 3) are close to those found when using chloroform/DPE.

After thermal annealing of 1′HD-PDPP3T:$PC_{71}BM$ blends, their TEM images shows a more phase-separated nanomorphology with lighter polymer-rich and darker fullerene-rich domains (Figure 6d,e). The change towards more pure domains reduces the EQE, especially in the wavelength range were the polymer absorbs light (Figure 5b). The change is very similar for both casting solvents. This can be understood by the fact that the increased phase separation reduces the interfacial donor-acceptor area where charges are created. Because of the short-exciton diffusion length, excitons created further than a few nanometers from the donor–acceptor interface do not contribute to charge generation. Upon annealing the FF decreases for the blends cast from chloroform/DPE (from 0.38 to 0.33), while the FF increase for blends cast from toluene/DPE increase (from 0.40 to 0.56). The higher contrast and the smaller feature size for the annealed toluene/DPE cast films compared to the chloroform/DPE cast films indicates higher purity domains for which charge carrier mobility can be higher result-

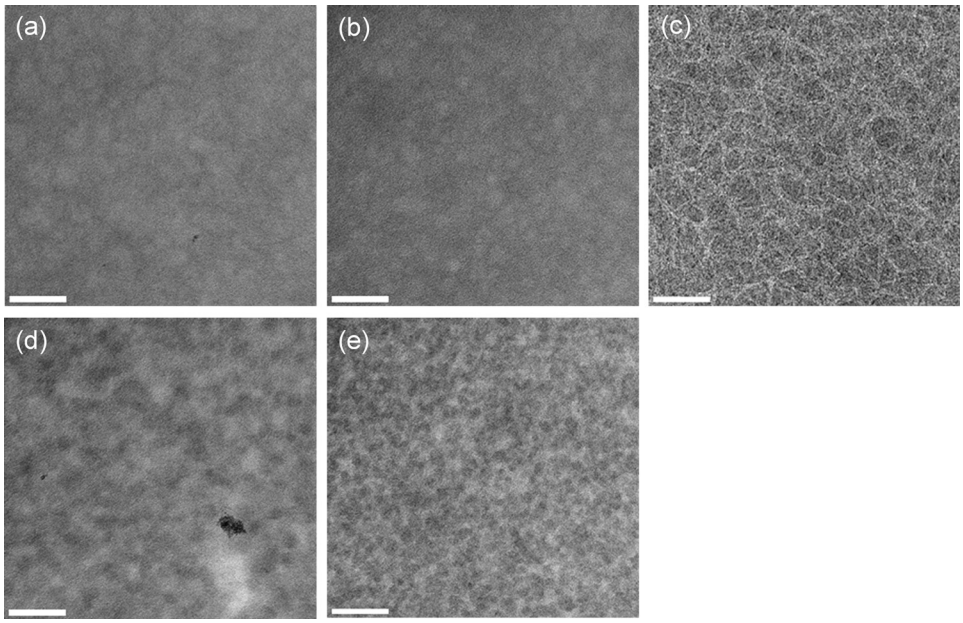

Figure 6. (a) TEM image of optimized 1′HD-PDPP3T:$PC_{71}BM$ blends cast from chloroform/DPE. (b) TEM image of optimized 1′HD-PDPP3T:$PC_{71}BM$ blends cast from toluene/DPE. (c) TEM image of optimized 2′HD-PDPP3T:$PC_{71}BM$ blends cast from chloroform/*o*-DCB.[17] (d) Same as (a) after thermal annealing at 150 °C for 30 s. (e) Same as (b) after thermal annealing at 150 °C for 30 s. White scale bars represent 100 nm.

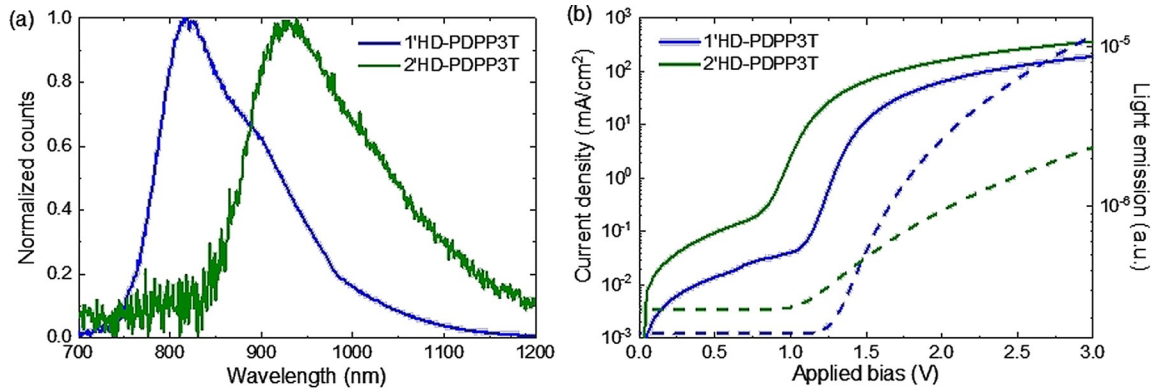

Figure 7. (a) Electroluminescence spectra of 1′HD-PDPP3T and 2′HD-PDPP3T based OLEDs. (b) Corresponding *J–V* characteristics for 1′HD-PDPP3T ($L = 85$ nm) and 2′HD-PDPP3T ($L = 65$ nm, solid lines) OLEDs and the simultaneously recorded *L–V* characteristics recorded with a Si photodiode (dashed lines).

ing in an improved FF. The reduced FF and V_{oc} for the annealed chloroform/DPE cast blends can at least in part be attributed to the reduced shunt resistance for these cells. The dark current (dashed light blue line in Figure 5 a) shows a substantial Ohmic contribution, indicating the presence of physical shunts. The bright region in Figure 6 d suggest that the film can be locally very thin in these blends.

Near infrared light-emitting diode

Light-emitting diodes were constructed by sandwiching 1′HD-PDPP3T and 2′HD-PDPP3T layers between ITO/PEDOT:PSS and LiF/Al electrodes. Figure 7 shows the electroluminescence spectra and current density–light intensity–voltage (*J–L–V*) characteristics. The electroluminescence emitted by 1′HD-PDPP3T maximizes at 820 nm while for 2′HD-PDPP3T the maximum emission is found at 930 nm (Figure 7 a).

The devices were characterized by recording the *J–L–V* characteristics by measuring the light output using a silicon photodetector positioned on top of the OLED. As expected from the lower band gap, the threshold voltage for light output is lower for 2′HD-PDPP3T than for 1′HD-PDPP3T. On the other hand, the light output of the 1′HD-PDPP3T devices is considerably higher. This is attributed to a reduced aggregation of the polymer which increases the luminescence quantum yield. The large difference in current density of the OLED and the Si detector, however, indicates a low external quantum efficiency (ca. 10^{-7}).

Conclusions

The properties of 1′HD-PDPP3T with α-branched side chains on the DPP units differ dramatically from the characteristics of the 2′HD-PDPP3T isomer with β-branched side chains. The branching at the α-position enforces an out-of-plane orientation of the alkyl side chains, which creates a strongly reduced tendency of the polymer to aggregate. Consequently, 1′HD-PDPP3T can be molecularly dissolved in common organic solvents, in contrast to 2′HD-PDPP3T which has limited solubility in chloroform and TCE but is virtually insoluble in other media. Because of branching at the α-position, the crystallinity of 1′HD-PDPP3T is much less than that of 2′HD-PDPP3T. By reducing the tendency to aggregate, the α-branched side chains create a wider optical band gap for 1′HD-PDPP3T in solution and thin films than for 2′HD-PDPP3T. Also, the electrochemical band gap of 1′HD-PDPP3T is higher. The increased π–π stacking distance of 4.36 Å for 1′HD-PDPP3T inferred from 2D-GIWAXS compared to 3.70 Å for 2′HD-PDPP3T, explains the one-order of magnitude lower hole mobility for the α-branched isomer.

Solar cells with 1′HD-PDPP3T as a donor and $PC_{71}BM$ as an acceptor are less efficient (PCE = 4.0 %) than cells based on 2′HD-PDPP3T and $PC_{71}BM$ (PCE = 7.1 %), primarily as consequence of a reduced EQE and FF. The open-circuit voltage, however, is higher and the minimal photon energy loss of 0.59 eV is close to the empirical threshold of 0.60 eV.[25] TEM analysis shows that 1′HD-PDPP3T:$PC_{71}BM$ blends possess an intimately mixed nanomorphology that prevents efficient charge separation and charge transport, explaining the reduced EQE and FF. Interestingly, the increased solubility of the polymer in common solvents allowed for devices made from a non-chlorinated solvent mixture. The low tendency of 1′HD-PDPP3T to aggregate enables a clear near infrared electroluminescence in thin solid films.

In conclusion by repositioning the hexyl substituent from the β to the α position on a decyl side chain of a DPP polymer, a completely different, isomeric polymer was obtained, having different structural, solubility, optical, and electronic properties. The combination of near infrared photovoltaic response and near infrared electroluminescence for single conjugated polymer is remarkable.

Experimental Section

All experimental details are given in the Supporting Information.

Acknowledgements

We thank Dr. Junyu Li for GIWAXS measurements and Dr. Fallon Colberts for TEM measurements. We acknowledge funding from the European Research Council (Grant Agreement No.

339031) and the NWO Spinoza prize awarded to R.A.J. Janssen by the Netherlands Organization for Scientific Research (NWO), and the Ministry of Education, Culture and Science (Gravity program 024.001.035).

Conflict of interest

The authors declare no conflict of interest.

Keywords: aggregation · light-emitting diodes · organic solar cells · polymer semiconductors · thin film

[1] T. Lei, J. Y. Wang, J. Pei, *Chem. Mater.* **2014**, *26*, 594.
[2] J. Mei, Z. Bao, *Chem. Mater.* **2014**, *26*, 604.
[3] Y. Yang, Z. Liu, G. Zhang, X. Zhang, D. Zhang, *Adv. Mater.* **2019**, *31*, 1903104.
[4] Z. Liu, G. Zhang, D. Zhang, *Acc. Chem. Res.* **2018**, *51*, 1422.
[5] C. R. Bridges, M. J. Ford, E. M. Thomas, C. Gomez, G. C. Bazan, R. A. Segalman, *Macromolecules* **2018**, *51*, 8597.
[6] K. Kawabata, M. Saito, N. Takemura, I. Osaka, K. Takimiya, *Polym. J.* **2017**, *49*, 169.
[7] H. J. Kim, M. Pei, J. S. Ko, M. H. Ma, G. E. Park, J. Baek, H. Yang, M. J. Cho, D. H. Choi, *ACS Appl. Mater. Interfaces* **2018**, *10*, 40681.
[8] Y. Deng, W. Li, L. Liu, H. Tian, Z. Xie, Y. Geng, F. Wang, *Energy Environ. Sci.* **2015**, *8*, 585.
[9] C. Cabanetos, A. El Labban, J. A. Bartelt, J. D. Douglas, W. R. Mateker, J. M. J. Fréchet, M. D. McGehee, P. M. Beaujuge, *J. Am. Chem. Soc.* **2013**, *135*, 4656.
[10] W. Li, K. H. Hendriks, M. M. Wienk, R. A. J. Janssen, *Acc. Chem. Res.* **2016**, *49*, 78.
[11] Y. Li, P. Sonar, L. Murphy, W. Hong, *Energy Environ. Sci.* **2013**, *6*, 1684.
[12] M. A. Naik, S. Patil, *J. Polym. Sci. Part A* **2013**, *51*, 4241.
[13] C. B. Nielsen, M. Turbiez, I. McCulloch, *Adv. Mater.* **2013**, *25*, 1859.
[14] A. Leventis, J. Royakkers, A. G. Rapidis, N. Goodeal, M. K. Corpinot, J. M. Frost, D.-K. Bučar, M. O. Blunt, F. Cacialli, H. Bronstein, *J. Am. Chem. Soc.* **2018**, *140*, 1622.
[15] F. Sugiyama, A. T. Kleinschmidt, L. V. Kayser, D. Rodriquez, M. Finn, M. A. Alkhadra, J. M.-H. Wan, J. Ramírez, A. S.-C. Chiang, S. E. Root, S. Savagatrup, D. J. Lipomi, *Polym. Chem.* **2018**, *9*, 4354.
[16] M. Grzybowski, D. T. Gryko, *Adv. Opt. Mater.* **2015**, *3*, 280.
[17] K. H. Hendriks, G. H. L. Heintges, V. S. Gevaerts, M. M. Wienk, R. A. J. Janssen, *Angew. Chem. Int. Ed.* **2013**, *52*, 8341; *Angew. Chem.* **2013**, *125*, 8499.
[18] M. Li, J. Li, D. Di Carlo Rasi, F. J. M. Colberts, J. Wang, G. H. L. Heintges, B. Lin, W. Li, W. Ma, M. M. Wienk, R. A. J. Janssen, *Adv. Energy Mater.* **2018**, *8*, 1800550.
[19] B. M. W. Langeveld-Voss, M. P. T. Christiaans, R. A. J. Janssen, E. W. Meijer, *Macromolecules* **1998**, *31*, 6702.
[20] F. Panzer, H. Bässler, A. Köhler, *J. Phys. Chem. Lett.* **2017**, *8*, 114.
[21] R. E. M. Willems, C. H. L. Weijtens, X. De Vries, R. Coehoorn, R. A. J. Janssen, *Adv. Energy Mater.* **2019**, *9*, 1803677.
[22] P. N. Murgatroyd, *J. Phys. D* **1970**, *3*, 151.
[23] J. C. Blakesley, F. A. Castro, W. Kylberg, G. F. A. Dibb, C. Arantes, R. Valaski, M. Cremona, J. S. Kim, J.-S. Kim, *Org. Electron.* **2014**, *15*, 1263.
[24] C. M. Proctor, M. Kuik, T.-Q. Nguyen, *Prog. Polym. Sci.* **2013**, *38*, 1941.
[25] W. Li, K. H. Hendriks, A. Furlan, M. M. Wienk, R. A. J. Janssen, *J. Am. Chem. Soc.* **2015**, *137*, 2231.
[26] F. Zhao, C. Wang, X. Zhan, *Adv. Energy Mater.* **2018**, *8*, 1703147.
[27] C. J. Brabec, M. Heeney, I. McCulloch, J. Nelson, *Chem. Soc. Rev.* **2011**, *40*, 1185.
[28] F. Liu, Y. Gu, X. Shen, S. Ferdous, H.-W. Wang, T. P. Russel, *Prog. Polym. Sci.* **2013**, *38*, 1990.
[29] W. Li, K. H. Hendriks, A. Furlan, W. S. C. Roelofs, S. C. J. Meskers, M. M. Wienk, R. A. J. Janssen, *Adv. Mater.* **2014**, *26*, 1565.
[30] W. Li, K. H. Hendriks, A. Furlan, W. S. C. Roelofs, M. M. Wienk, R. A. J. Janssen, *J. Am. Chem. Soc.* **2013**, *135*, 18942.
[31] J. J. Van Franeker, G. H. L. Heintges, C. Schaefer, G. Portale, W. Li, M. M. Wienk, P. Van der Schoot, R. A. J. Janssen, *J. Am. Chem. Soc.* **2015**, *137*, 11783.

Manuscript received: April 8, 2020
Revised manuscript received: May 21, 2020
Accepted manuscript online: May 26, 2020
Version of record online: September 29, 2020